A Study of the Extratropical Reintensification of Former Hurricane Earl Using Canadian Meteorological Centre Regional Analyses and Ensemble Forecasts

SUHONG MA,[*] HAROLD RITCHIE,[+] JOHN GYAKUM,[#] JIM ABRAHAM,[+] CHRIS FOGARTY,[@]
AND RON MCTAGGART-COWAN[#]

[*]National Meteorological Centre, Beijing, China
[+]Meteorological Service of Canada, Environment Canada, Dorval, Quebec, Canada
[#]Department of Atmospheric and Oceanic Sciences, McGill University, Montreal, Quebec, Canada
[@]Meteorological Service of Canada, Newfoundland Weather Centre, Gander, Newfoundland, Canada

ABSTRACT

Former Hurricane Earl reintensified rapidly while traveling through Canadian waters in September 1998. Its central pressure decreased 40 hPa over a 36-h period, and it produced heavy rain on Cape Breton Island, Nova Scotia, and over Newfoundland. A diagnostic study is conducted from a potential vorticity (PV) perspective using Canadian Meteorological Centre (CMC) regional analysis data. Former Hurricane Earl's rapid redevelopment was related to the interaction between two preexisting positive PV anomalies: a diabatically generated low-level anomaly and an upper-level anomaly. This process was accompanied by a cold air intrusion and warm air "wrapping up" process. As well, the behavior of the operational CMC numerical weather prediction models is examined using output from the ensemble forecast system (giving 10-day forecasts, with eight members and one control run) integrated from three different initial times (0000 UTC on each of 3, 4, and 5 September 1998). Some members failed to maintain former Hurricane Earl's observed closed cyclonic circulation during the weakening period, and subsequently developed only a weak low pressure system. Others maintained the identity of former Hurricane Earl throughout both the weakening and reintensifying periods. Static PV inversions suggest that the more successful forecasts of Earl's reintensification were associated with preferentially strong lower-tropospheric cyclonic circulations induced by the upstream upper-tropospheric PV maximum. This induced lower-level flow also produced the very large-amplitude low-level thermal perturbations characteristic of a deepening baroclinic low.

1. Introduction

Tropical cyclones that develop in the Atlantic Ocean during the late summer and autumn months often move over colder waters into middle and northern latitudes after recurvature. They are normally in their decay stage, and their translation speeds are increasing under the influence of the midlatitude westerly circulation (Anthes 1982).

Of the eight tropical cyclones that form in the Atlantic Ocean each year on average (Holland 1993), two or three of these can be expected to impact weather in Atlantic Canada (Joe et al. 1995) and often bring very heavy rains and strong winds. Storms that have recently affected Atlantic Canada include landfalling hurricanes such as Hortense (September 1996) in Nova Scotia (Pasch and Avila 1999) and Luis (September 1995) in Newfoundland (Lawrence and Mayfield 1998). Tropical

systems need not make landfall to unleash their fury over land. Hurricane Beth brought heavy rains (>250 mm) to mainland Nova Scotia in August 1971 while tracking across eastern Nova Scotia. The remains of Hurricane Hugo tracked well north of Atlantic Canada in September 1989, yet brought high winds to much of the area.

Tropical cyclones threatening the United States and the Caribbean receive significant international media attention. While this raises the awareness level of the Canadian public, there can be some confusion as to the exact nature of the threat that these storms might later pose to Canada, and subsequently to the North Atlantic and to Europe (Walmsley 1993). The strong winds, heavy rains, storm surge, and large waves are seldom at the same intensities as when the tropical cyclone was farther south. However, there remains a problem unique to the middle latitudes—that of a potential rapid reintensification of the cyclone interacting with a preexisting weather system—an explosive extratropical transition (ET).

Only a few ET cases have been studied in the past. Perhaps the worst natural disaster in Canadian history

Corresponding author address: Harold Ritchie, Meteorological Service of Canada, Environment Canada, 5th Floor, 2121 Trans-Canada Hwy., Dorval, QC H9P 1J3, Canada.
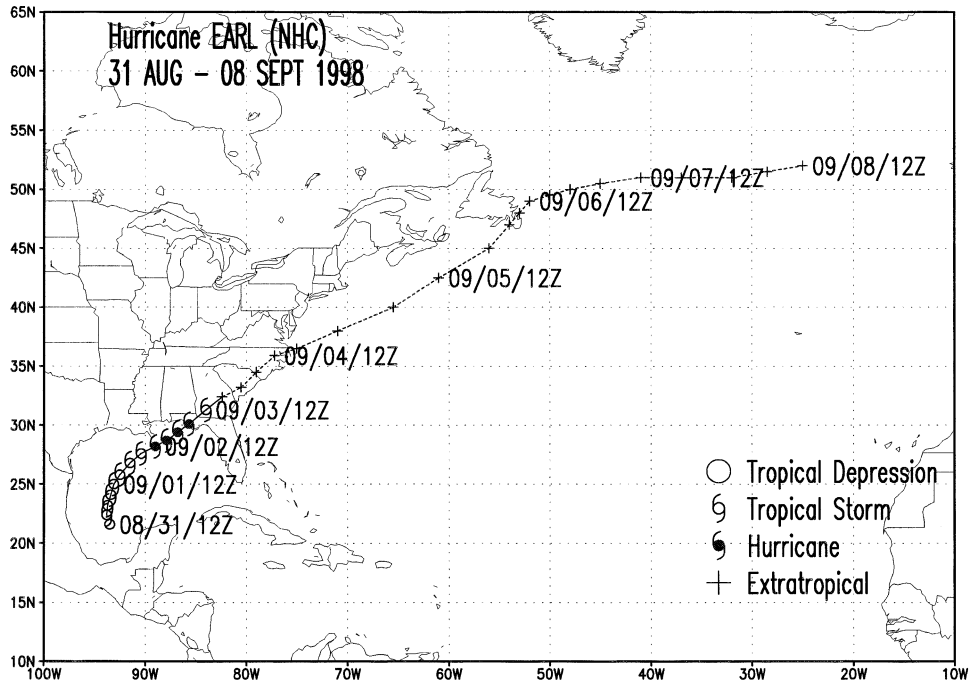E-mail: hal.ritchie@ec.gc.ca

FIG. 1. The NHC best track (6-h positions) for Earl from 1200 UTC 2 Sep to 1200 UTC 8 Sep.

occurred as a result of a hurricane that killed as many as 4000 mariners off the coast of Newfoundland in 1775 (Jones 1990). Certainly the most famous hurricane in modern days in Canada was Hazel, which killed 83 people in southern Ontario in October 1954 (Knox 1955; Palmén 1958). Two of the 10 costliest hurricanes in the United States were associated with storms in transition. The Hurricane of 1938 (Pierce 1939) was the costliest storm to that date and resulted in over 600 deaths. DiMego and Bosart (1982) analyzed the ET and subsequent reintensification of the infamous Agnes case in June of 1972 that resulted in 129 deaths and $3.5 billion in damage to property (1972 dollars). Much of this devastation was a result of the extensive flooding caused by extremely heavy rainfalls of 200–300 mm in less than 1 day. Sinclair (1993) studied precipitation over New Zealand resulting from the transition of Tropical

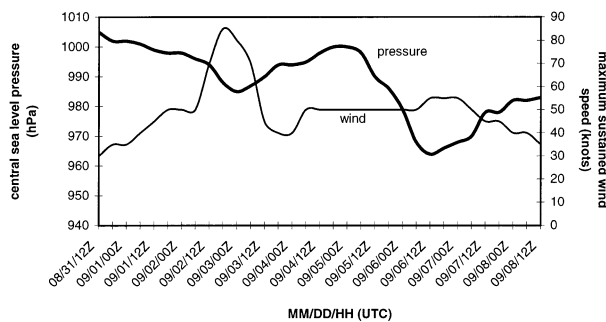

FIG. 2. Plots of minimum central SLP (heavy solid) and maximum sustained wind speed determined using the U.S. 1-min average method (light solid).

Cyclone (TC) Bola in March of 1988, and Foley and Hanstrum (1994) studied the capture and transition of tropical cyclones in Australia. More recently, Browning et al. (1998) have analyzed the role of upper- and lower-level potential vorticity (PV) interaction and intrusion of dry tropospheric air into the circulation of ex–Hurricane Lili in October of 1996. Thorncroft and Jones (2000) have examined transitioning storms as they crossed the Atlantic, and Klein et al. (2000) have provided an overview of ET in the western North Pacific. A climatology of ET in the Atlantic basin is presented by Hart and Evans (2001). They found that 40% of all tropical cyclones in the Atlantic basin underwent ET and the transition most often occurred at lower latitudes (30°–35°N) early and late in the hurricane season, and at high latitudes (40°–50°N) in the peak hurricane season. Around 50% of the posttransition intensity change variability can be described by the transit time a tropical cyclone requires to enter the region where extratropical development is supported after leaving the tropically supportive region. Both weak and strong tropical cyclones can intensify after transition; however, weak tropical cyclones (central mean sea level pressure >990 hPa) must enter a baroclinically supportive region soon (<20 h) after leaving a tropically supportive region if posttransition intensification is going to occur.

In early September 1998, the remnants of Hurricane Earl led to an intense extratropical storm that ravaged eastern Nova Scotia and Newfoundland with 50–100-mm rainfalls and that contained sustained offshore winds of 25 m s^{-1} (50 kt). Figure 1 shows the track and life history of Earl as analyzed by the National Hurri-
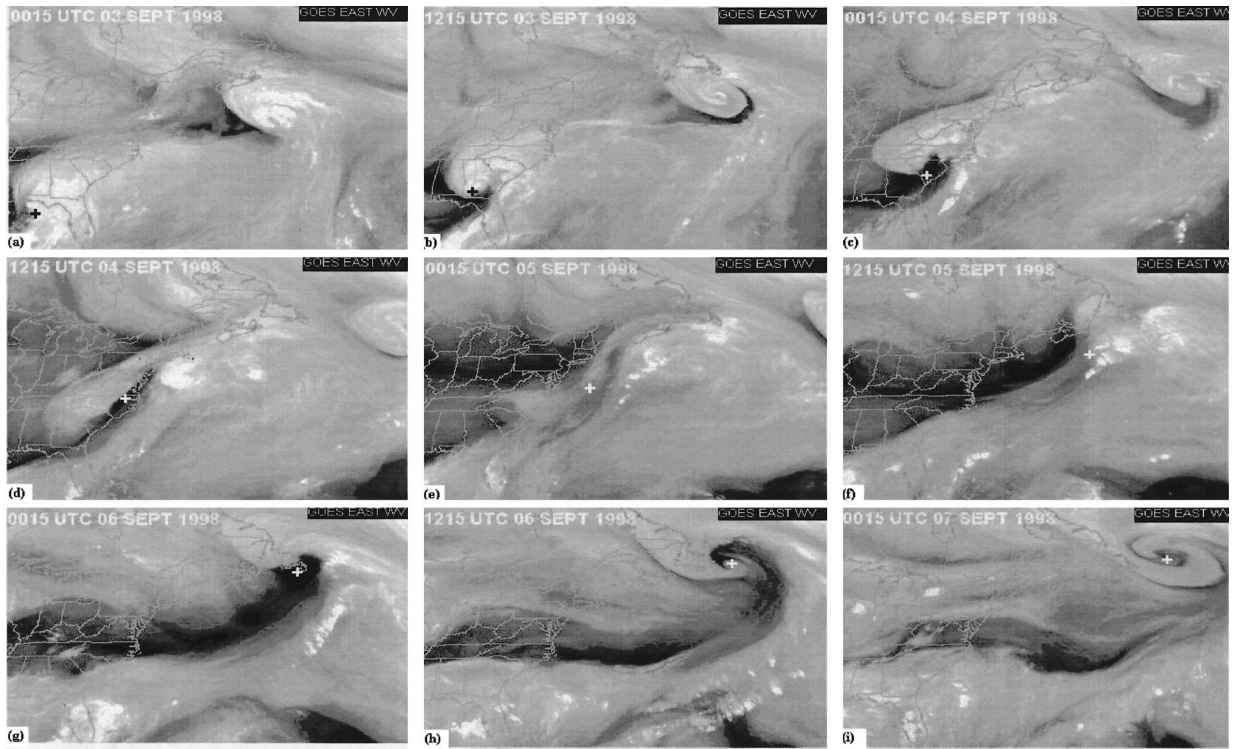
Fig. 3. *GOES-East* water vapor imagery from 0015 UTC 3 Sep to 0015 UTC 7 Sep.
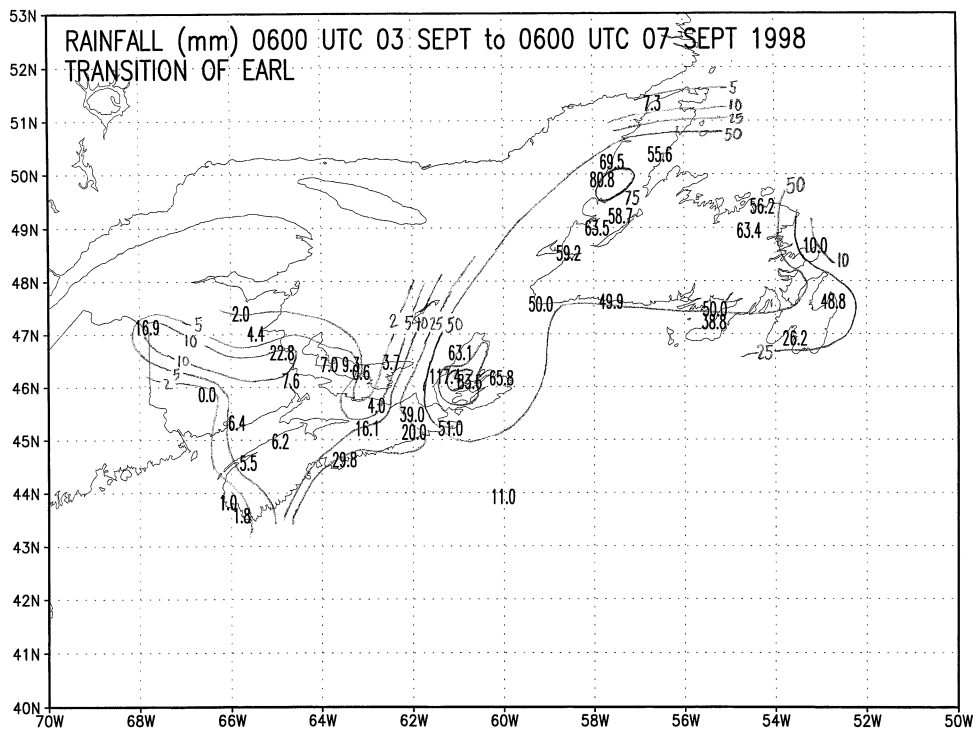

Fig. 4. Rainfall (mm) over the Atlantic provinces from 0600 UTC 3 Sep to 0600 UTC 7 Sep.

TABLE 1. Options characterizing the ensemble members (based on Houtekamer et al. 1997). GWD refers to gravity wave drag. The ∇^8 diffusion *e*-folding times (h) are for wavenumber 63. ACARS–AMDAR refers to the automated aircraft wind observations obtained from commercial aircraft.

Model no.	∇^8 diffusion *e*-folding time (h)	Convection radiation	GWD	GWD version	Orography	ACARS–AMDAR obs	Addition to operational analysis
1	29	Kuo/Garand	Strong	High altitude	0.3 envelope	Yes	Yes
2	29	Manabe/Sasamori	Strong	Low altitude	0.3 envelope	No	No
3	29	Kuo/Garand	Weak	Low altitude	Mean	Yes	No
4	29	Manabe/Sasamori	Weak	High altitude	Mean	No	Yes
5	58	Manabe/Sasamori	Strong	Low altitude	Mean	Yes	Yes
6	58	Kuo/Garand	Strong	High altitude	Mean	No	No
7	58	Manabe/Sasamori	Weak	High altitude	0.3 envelope	Yes	No
8	58	Kuo/Garand	Weak	Low altitude	0.3 envelope	No	Yes

cane Center (NHC) (Mayfield 1999). A study of this ET/reintensification event forms the basis of this paper. Hurricane Earl's evolution followed a pattern similar to that of Hurricane Hazel (Palmén 1958) in 1954 and Tropical Storm Agnes (Simpson and Hebert 1973) in 1972. These storms were studied in the context of a two-phase transition process. The first (tropical dissipation) period occurred as the tropical cyclone made landfall, moved inland, and weakened. The second stage began as the weakened tropical system interacted with a strong baroclinic zone and upper-level trough in the midlatitudes. Klein et al. (2000) have developed a conceptual model, with the ET process initiated as the poleward moving TC responds to changes in its environment (the "transformation stage"). Subsequently the system develops the characteristics of a midlatitude storm (the "extratropical" or "reintensification stage").

The goals of the present paper are (i) to document the stages associated with the extratropical transition of Earl, (ii) to study the reintensification of Earl using an Ertel PV framework (Ertel 1942), and (iii) to analyze the performance of numerical models through examination of the ensemble forecast system of the Canadian Meteorological Centre (CMC). As well, the CMC regional analysis fields will be used to diagnose the synoptic environment during Earl's reintensification phase.

Interest in many of these reintensifying ex–tropical storms is justified by the fact that their deepening rate and their speed of forward motion are similar to severe winter storms [the so-called bombs described by Sanders and Gyakum (1980)], but occurring in the late summer or autumn when numerous small fishing and recreational craft are at sea. Furthermore, these storms present a significant threat to populated areas in the form of heavy rainfall and the potential for flash flooding.

An overview of the life history of Earl (section 2) is followed by a description of the data and methodology (section 3), diagnostics based on the CMC regional analyses (section 4), a diagnosis of the CMC ensemble forecasts (section 5), and a summary and conclusions (section 6).

2. Storm overview

Hurricane Earl began as a small-amplitude Cape Verde easterly wave whose development was suppressed by the outflow from Hurricane Bonnie as it moved across the tropical Atlantic Ocean. As a result, Earl did not intensify to tropical depression status until it reached the Gulf of Mexico on 31 August 1998. Earl's winds quickly reached tropical storm strength (maximum sustained surface winds of at least 18 m s^{-1}) as the system moved north-northeastward on 1 September, and later northeastward as a hurricane with maximum sustained winds near 40 m s^{-1} on 2 September. After making landfall as a marginal hurricane (winds of 34 m s^{-1}) on the Florida panhandle, the storm crossed Georgia and the Carolinas, and was declared extratropical by the NHC at 1800 UTC 3 September. The weakening extratropical storm headed toward Sable Island off Nova Scotia on 5 September and by 1200 UTC had begun to reintensify. The heavy solid curve in Fig. 2 shows the trace of minimum central sea level pressure (SLP) as recorded by the NHC. The lowest SLP (964 hPa) occurred at 1200 UTC on 6 September just after the storm's passage over Newfoundland's Avalon Peninsula. Thereafter, the system weakened and moved in an easterly direction just north of 50°N. The light solid curve in Fig. 2 shows the evolution of the maximum sustained wind speed. As can be seen from the SLP trace in Fig. 2 and the 6-h positions in the NHC best track (Fig. 1), the period of reintensification was associated with a rapid acceleration of the storm as it interacted with an upper-level trough. In a model sensitivity study using PV inversions to modify initial conditions for this case, McTaggart-Cowan et al. (2001) have found that the existence of this trough is of primary importance to the storm's reintensification. As discussed later, there are suggestions that there may have actually been a secondary cyclone development during the reintensification, casting some doubt on the NHC track positions between 0000 and 0600 UTC 5 September.

a. Satellite imagery

Figure 3 displays the evolution of Geostationary Operational Environment Satellite (*GOES-East*) water vapor imagery from 0000 UTC 3 September to 0000 UTC 7 September. These images capture the two phases dis-
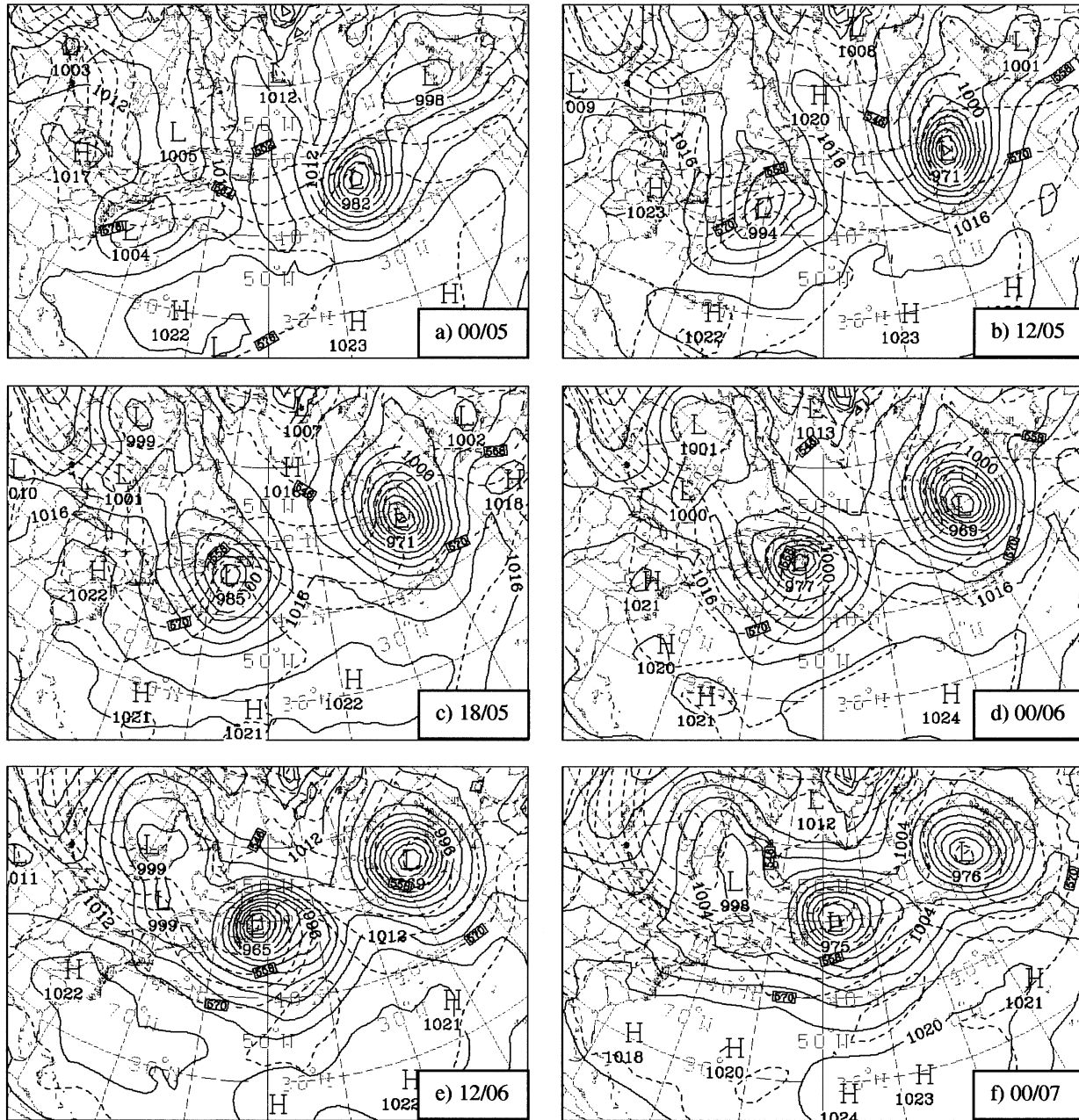
FIG. 5. Sea level pressure (solid contours) with a 4-hPa contour interval, and 1000–500-hPa thickness at 4-dam increments (dashed contours), from 0000 UTC 5 Sep to 0000 UTC 7 Sep.

cussed earlier by Klein et al. (2000), namely the 48-h tropical decay period (transformation stage) from 0000 UTC 3 September to 0000 UTC 5 September and the 36-h extratropical transition reintensification stage between 0000 UTC 5 September and 1200 UTC 6 September. By 0000 UTC 3 September, Earl displays an asymmetric cloud atypical for a hurricane. After moving well inland and becoming extratropical 18 h later, a hook cloud pattern is well defined with a trailing cold-frontal feature off the Atlantic Coast. The separate system east of Newfoundland is the remnant of Hurricane Danielle,

which is also undergoing ET. During the weakest stage of Earl between 1200 UTC 4 September and 0000 UTC 5 September, the main cloud field becomes significantly displaced to the east of the center and merges with a new frontal wave south of Nova Scotia. Significant deepening has occurred by 1200 UTC 5 September as a new area of cloudiness forms north of the center over Newfoundland and the eastern Gulf of St. Lawrence. This area of cloudiness is evidence suggesting that secondary cyclogenesis has occurred. During the most intense period on 6 September, a strong comma-shaped
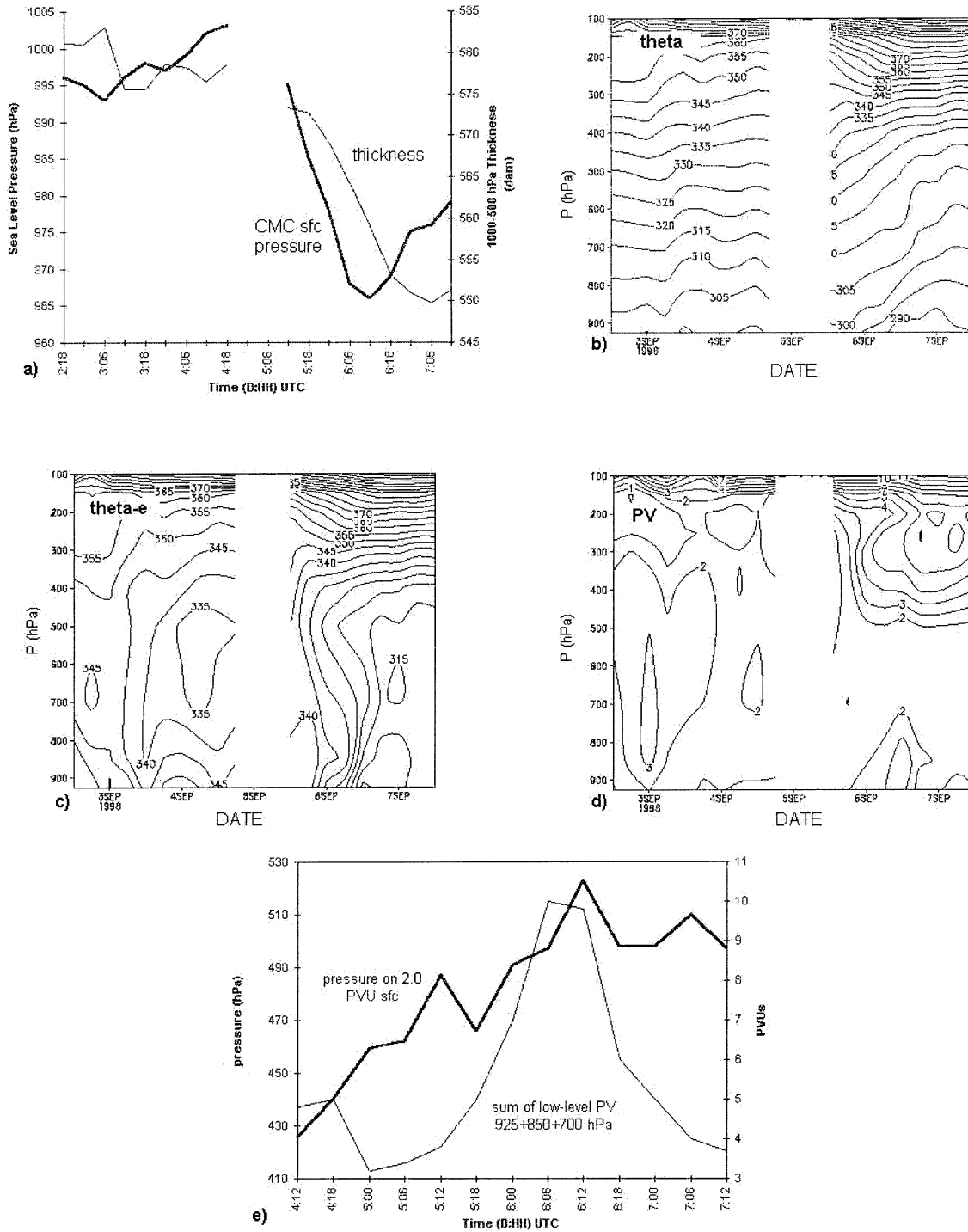
FIG. 6. Life history of Earl. (a) Time series of 1000–500-hPa thickness (thin line, dam) and minimum CMC SLP (thick line, hPa). (b) Time–height plots of potential temperature (theta) with a contour interval of 5 K. (c) Equivalent potential temperature (theta-e), again with an interval of 5 K, and (d) Ertel's PV in 1-PVU increments. All of the above panels are plotted from 1200 UTC 2 Sep to 1200 UTC 7 Sep with the omission of 0000 and 0600 UTC 5 Sep. (e) Time series of the maximum pressure on the 2-PVU surface (thick line, hPa) and the summed maximum low-level (925, 850, and 700 hPa) PV (thin line, PVU) from 1200 UTC 4 Sep to 1200 UTC 7 Sep.
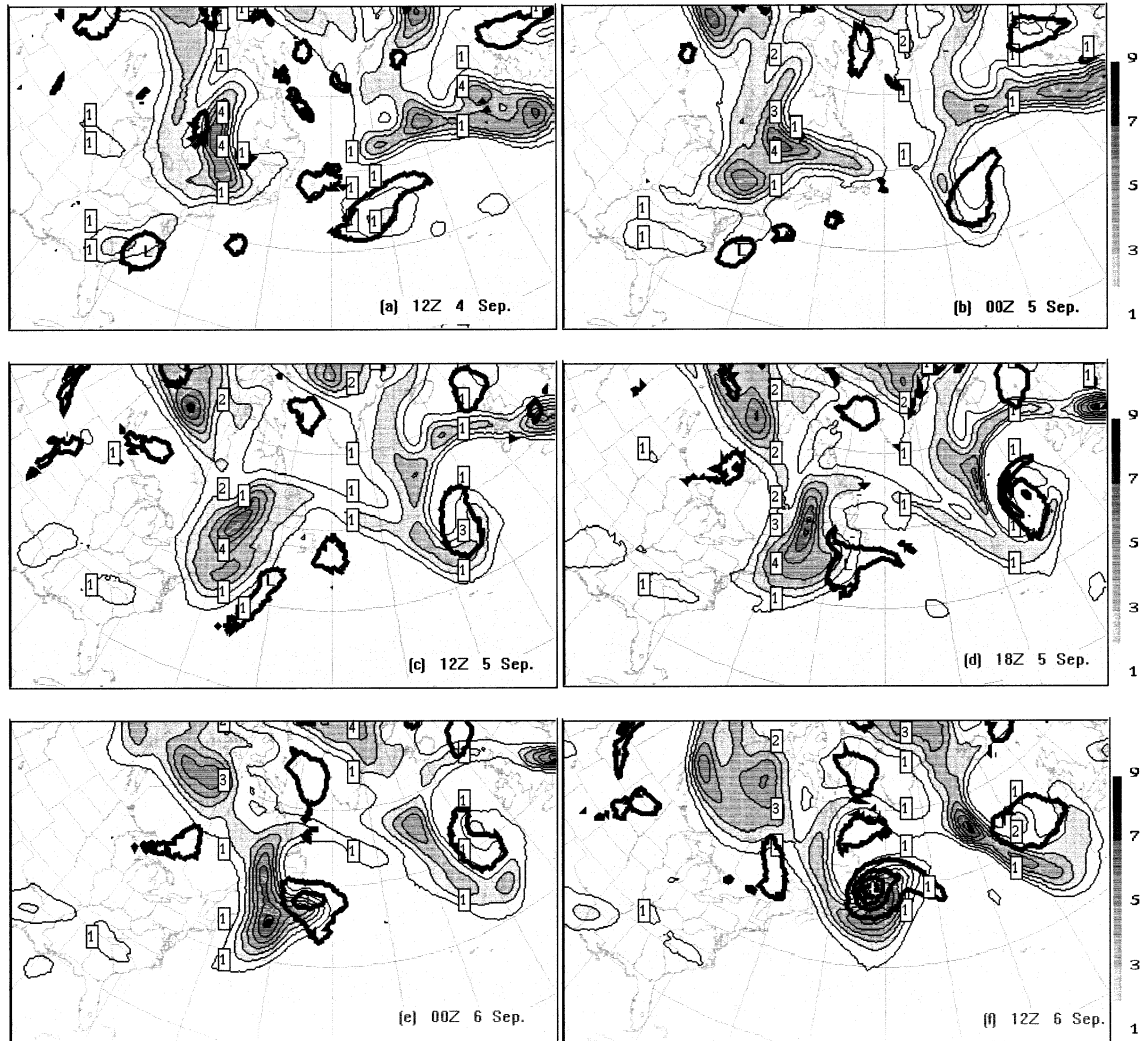
FIG. 7. The PV at 300 (thin contours and shading) and at 850 hPa (thick contours), both with 1-PVU contour intervals from 1200 UTC 4 Sep to 1200 UTC 6 Sep. The location of Earl is indicated by a boldface L (black or white).

pattern forms with a hook wrapping around the cyclone center (964 hPa) at 1200 UTC 6 September. A spiraling cloud pattern centered about the cyclone marks the beginning of the decay on 7 September.

As Earl underwent ET on 3 and 4 September, dry air from the north and west was invading the storm's center, forming a familiar dry slot like that which is often seen in mature extratropical cyclones. Vertical wind shear could also be associated with the dry slot. As a consequence, there was a loss of convection over the center and the storm weakened rapidly. Much of the remaining moisture was displaced to the northeast as the remains of Earl moved toward the North Carolina coast on 4 September. On 5 September a belt of dry air moved off the coast of North America and close to the center of the storm. This belt wrapped around the eastern periphery of the circulation early on 6 September, even-

tually enclosing the center as the storm weakened later that day.

b. Observed rainfall

Data from a network of rain gauges (Fig. 4) were used to determine the distribution of rainfall over the Atlantic provinces from 0600 UTC 3 September to 0600 UTC 7 September. The data were obtained from the Meteorological Service of Canada climate station database in Fredericton, New Brunswick. It was found that precipitation from Hurricane Danielle (initially near Newfoundland) did not contaminate the 4-day "Earl period" totals in Fig. 4. Before the remains of Earl neared the coasts of Nova Scotia and Newfoundland, light amounts of precipitation were recorded owing to the presence of a weak frontal system. However, the
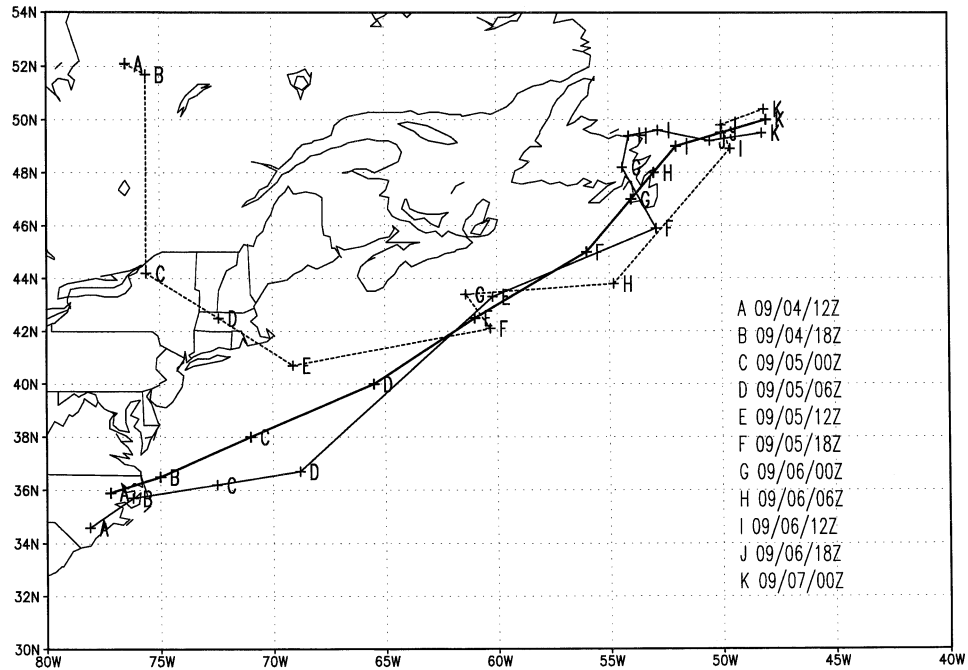
FIG. 8. Tracks of upper-level PV maximum [maximum pressure (hPa) on the 2-PVU surface (thin dashed)] and low-level PV anomaly [summed low-level potential vorticity (PVUs) of the 925-, 850-, and 700-hPa levels (thin solid)] for the times A–K shown in the legend. Thickest line shows the NHC best track.

majority of the precipitation fell during 5 and 6 September and was associated with Earl's passage.

The heaviest precipitation fell over Nova Scotia's Cape Breton Island and most of Newfoundland except for the extreme northern part of the island. Satellite imagery (Fig. 3) indicates a detached area of cloudiness moving from Cape Breton to Newfoundland on 5 Sep-
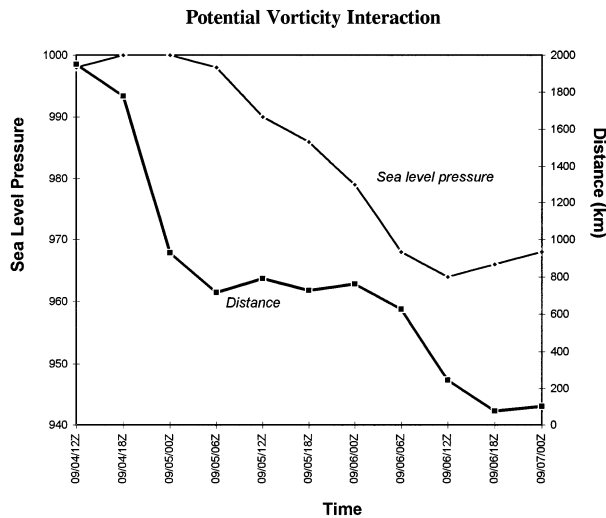

FIG. 9. The time series of the interaction distance (km)—as defined by the horizontal separation between the location of the maximum pressure on the 2-PVU surface and the location of the low-level PV anomaly at 925 hPa—is plotted as the thick curve. The thin curve represents the NHC analysis of SLP in hPa.

tember. Orographic features explain the local peaks in rainfall observed at Cow Head, Newfoundland (81 mm), and at Inverness, Nova Scotia (117 mm). Sinclair (1993) also observed such significant orographically induced peaks in the rainfall patterns from TC Bola in New Zealand. Near the storm track in eastern Newfoundland lesser amounts were observed due to the close proximity of the dry slot wrapping around the storm's center at the time.

3. Data and methodology

The PV perspective will be applied to diagnose the reintensification of the weather system once known as Hurricane Earl. In a hydrostatic atmosphere and in isobaric coordinates, PV can be expressed as

$$\mathrm{PV} = -g\frac{\partial \theta}{\partial p}\left(f + \frac{\partial v}{\partial x} - \frac{\partial u}{\partial y}\right) + g\left(\frac{\partial v}{\partial p}\frac{\partial \theta}{\partial x} - \frac{\partial u}{\partial p}\frac{\partial \theta}{\partial y}\right), \quad (1)$$

where the symbols have their usual meaning. It is worth noting that the first three terms on the right-hand side are much larger than the other terms involving the baroclinic and horizontal vorticity components.

A definition of the tropopause in terms of PV is more useful than a lapse rate definition (Hoskins et al. 1985). In this study a 2.0-PVU surface is defined as the dynamic tropopause (PVU is the unit for PV, 1 PVU = 1.0×10^{-6} K m^2 kg^{-1} s^{-1}), which approximates the boundary between the smaller PV magnitudes of the troposphere and the larger cyclonic PV reservoir of the

stratosphere. A positive upper-level PV anomaly in the Northern Hemisphere typically corresponds to a cyclonic vorticity maximum, and a physically lower dynamic tropopause. A positive lower-tropospheric PV anomaly typically occurs as a result of an upward increase in latent heating. A positive potential temperature anomaly near the surface is a surrogate for a positive PV anomaly. Here an anomaly is defined as the difference of the full value and the time mean (e.g., the 18-day average).

In section 4, CMC regional analysis data will be used on a polar stereographic grid, with a horizontal resolution of 35 km at 60°N and 16 pressure levels up to 10 hPa. These data will be used in the diagnostic computations of geopotential thickness, PV, potential temperature, and equivalent potential temperature over a domain of 240 × 140 grid points.

In section 5, we will present results based on the CMC ensemble forecast system. In its 1998 operational version, the CMC ensemble forecasting system consists of eight members and one control, all of which represent different configurations of the spectral model referred to as the Spectral Éléments Finis (SEF; Ritchie and Beaudoin 1994). The model uses T95 truncation, which corresponds to a grid spacing of approximately 1.875° latitude. Outputs are examined on 14 mandatory standard pressure levels, on a domain with 45 × 29 grid points, which is approximately the same area as that of the regional analysis data. All eight members and the control run have the same horizontal resolution, but they have different vertical resolution (e.g., members 1, 3, 5, 7 have 23 vertical levels and members 2, 4, 6, 8 have 41 vertical levels) and different time integration schemes (e.g., some members use a three-time-level integration scheme, and some use a two-time-level integration scheme). They all run from different perturbed analyses and use different physical process parameterization schemes, such as different convection (Kuo or Manabe), radiation (Garand or Sasamori), and gravity wave drag schemes. They also have different representations of orography. The combinations of these options that characterize the members are summarized in Table 1 [for more detail see Houtekamer et al. (1996) and Houtekamer and Lefaivre (1997)].

As explained in section 2 of Houtekamer et al. (1996), the perturbed analyses are generated using the "breeding growing modes" approach. Here all elements of the forecasting system are considered to be subject to error or imperfection. The model errors are reflected by the use of the different combinations of realistic model options as explained above. In order to reflect the uncertainty in the initial conditions for the forecasts, each model configuration is used in a continuously running 6-h intermittent data assimilation cycle. Here we outline the procedure based on model configuration *i*. For data assimilation cycle *i,* the input observations are randomly perturbed in agreement with their error statistics. Applying the analysis step yields perturbed analysis *i,* which is then integrated with model version *i* to produce a 6-h forecast that serves as the first guess for the assimilation of the next set of perturbed observations. Note that the first guess perturbation contains a contribution from model error (reflected by the model options that characterize model version *i* vs the options used in the other cycles) and from observational error (reflected by the random perturbations to the observations in agreement with their error statistics) that have evolved during 6 h with the model dynamics. As the cycling proceeds, the difference patterns among the various cycles reflect the weaknesses of the model and the observing system as well as characteristics of the dynamics. These difference patterns will tend to grow in time due to the growth of the model forecast errors. But their growth is also limited by the assimilation of realistically perturbed observations, so that the difference patterns will become dominated by the most rapidly growing modes that are characteristic of the current atmospheric dynamics. Hence this procedure breeds growing modes. Integrating perturbed analysis *i* for 10 days using model version *i* generates one member of the ensemble of forecasts.

In this way, the ensemble forecasts represent an attempt to estimate the full range of possible outcomes given a realistic range of possible initial conditions (together with equally good model configurations). The results have been assessed in terms of verification of the mean forecast and the control run. This is usually carried out by calculating the root-mean-square errors for the ensemble mean and the control run with respect to the analysis. We expect that, on average, the mean track of the ensemble members will agree better with observations than will the track from the control (Zhang and Krishnamurti 1999).

In section 5, we will take advantage of the variability of the ensemble results to study the behavior of the individual ensemble members and present some statistical results to demonstrate which factors may be important for the strong reintensification of ex-Earl.

In the present study we use the CMC ensemble forecasting system to produce 10-day forecasts from three different initial times: 0000 UTC on 3, 4, and 5 September. The integrations initialized at 0000 UTC on 3 and 4 September simulate both the weakening and reintensification stages of Earl. Integrations initialized at 0000 UTC 5 September only simulate the reintensification period.

4. Diagnostics using the CMC regional analyses

a. Storm evolution

Sea level pressure and 1000–500-hPa geopotential thickness fields during the reintensification period of the former Earl are displayed in Fig. 5. The weakening remnants of Earl have been moving east-northeastward off the New Jersey coast, with a surface trough extending

northeastward over the Maritime Provinces. Explosive reintensification has begun by 1200 UTC 5 September (Fig. 5c) when Earl merges with the trough and with the strong troposphere-deep baroclinic zone to the northwest. The upper-level trough to the northwest (and its associated PV anomaly) is a key factor in the reintensification since it provides an environment conducive to cyclogenesis. The shape of the 1008-hPa contour in Fig. 5b is a further suggestion that a secondary extratropical cyclone formed in this environment several hundred kilometers to the northeast of the former Earl at approximately 1800 UTC 4 September.

The mature phase of this warm-core ''seclusion'' process (Shapiro and Keyser 1990) is evidenced in Fig. 5e by a wrapping up of the thickness field. After 1200 UTC 6 September (Fig. 5f) the former Earl is entering the decay phase.

Figures 6a–e show the time evolution of the system from decay through reintensification. The values of potential temperature, equivalent potential temperature, and PV over the center (Figs. 6b–d, respectively) are calculated as the arithmetic means of the 5×5 grid points around the surface center (a region of about 140 km $\times$ 140 km). The center is defined as the location of the local minimum in sea level pressure in the CMC analysis.

As Earl moved northeastward during the period from 1800 UTC 4 September to 1200 UTC 5 September a secondary low may have formed to the northeast. The position of the pressure center(s) becomes ambiguous for 0000–0600 UTC 5 September given the elongated trough in the surface pressure field. Therefore we do not compute the storm-centered diagnostics for these two times, even though the NHC maintained Earl as a separate center.

Figures 6a and 6b show that during the weakening (transformation) stage, the former Earl maintained its warm-core structure, with 1000–500-hPa thicknesses over the center ranging between 575 and 580 dam. In Fig. 6c the layers of potential instability prior to reintensification correspond well with the location of low-level PV anomalies shown in Fig. 6d.

The onset of reintensification is well correlated with a decrease in the 1000–500-hPa thicknesses, a drop in height of the dynamic tropopause, and an increasingly stable stratification of the troposphere above the cyclone. The significant drop in thickness after 1200 UTC 5 September is shown in Fig. 6a. After the disintegration of the low-level PV anomaly in Fig. 6d, the cyclone weakens almost as rapidly as it intensified. Figure 6e shows the entire process in terms of the magnitude of the PV anomalies and highlights the importance of their coexistence in the intensification. This storm evolution is consistent with the general behavior described by Hart and Evans (2001). In particular, the reintensification of Earl at these latitudes during the peak hurricane season illustrates the importance of the interaction of the baroclinic region and the sea surface temperatures (SSTs).

Earl did decay while moving over a region of cooler SST, but the baroclinic zone moved in quickly enough to trigger the reintensification.

b. PV overview

In this section we analyze the reintensification of Earl in more detail using a PV approach (Hoskins et al. 1985). The use of PV in meteorology was first introduced by Rossby (1940), and its popularity has recently grown because of its attractive properties of conservation and invertability. It is now well known that the combination of low-level warm advection and an upper-level PV anomaly can result in strong cyclogenesis, with the magnitude of the effect depending on the relative positions of the anomalies. If the upper-level PV anomaly stays near the rear of the low-level warm anomaly (usually with a large positive low-level PV value), the wind field induced by it can result in mutual intensification. Low-level PV is often used as a ''surrogate'' for the low-level warm anomaly (Lackmann et al. 1996). It is thus helpful to look at the relationship between the upper- and lower-level PV anomalies in order to study Earl's reintensification. For this discussion, we ignore the anomalies over the central and eastern North Atlantic Ocean since they are associated with the transition of former Hurricane Danielle.

In Fig. 7a Earl's remnants appear as a single closed contour of 1 PVU over the Carolinas. A strong upper-level positive PV anomaly appears over Ontario and Quebec. At 0000 UTC 5 September (Fig. 7b) the upper anomaly elongates and intensifies, and a family of low-level PV anomalies, aligned southwest to northeast ahead of the trough, suggests convective instability in the region and perhaps the presence of a secondary cyclone southeast of Cape Cod, as suggested in the previous subsection. McTaggart-Cowan et al. (2001) discuss the important role of latent heat release in fueling an increase in PV due to convective precipitation near the cyclone center during the reintensification.

At the onset of reintensification near 1200 UTC 5 September (Fig. 7c), the upper-level PV anomaly is positioned well to the west of the low-level anomaly. The rapid filamentation and southeasterly extension of the upper-level PV maximum are associated with the digging of the trough as it moves across the East Coast. The rapid cyclonic roll-up of the upper-level PV anomaly is indicative of life cycle 2 (LC2)-type baroclinic development (Thorncroft et al. 1993) associated with a cyclonic Rossby wave break event. The largest stratospheric intrusions during such a rapid upper-level development typically occur at the southeastern edge of the PV anomaly. Further, the southeastward propagation of the filamenting anomaly places Earl's remnant in an ideal location for cyclogenesis after 1200 UTC 5 September. Intensification of the near-surface circulation continues as the anomalies interact by wrapping around each other as shown in Figs. 7d–f. When the storm
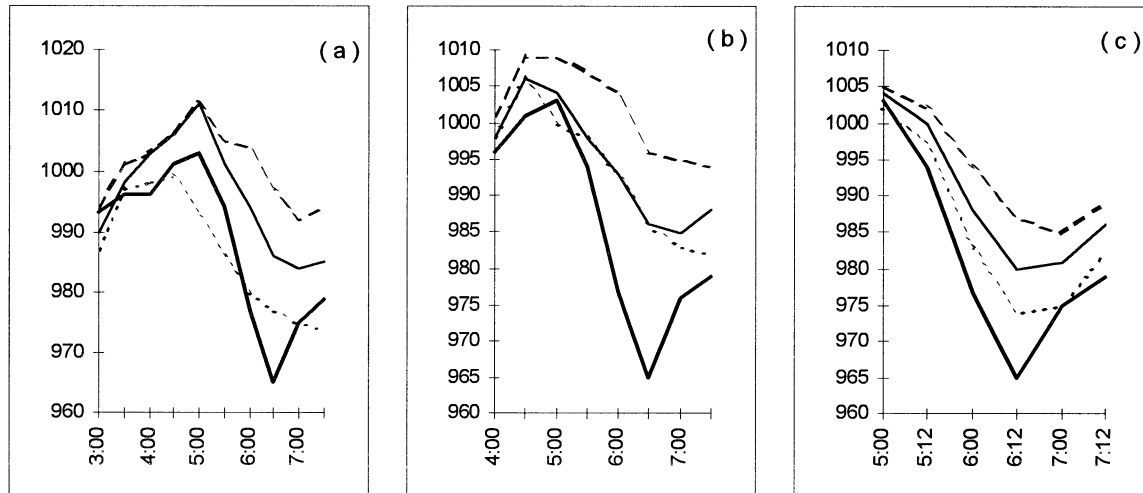
FIG. 10. The time evolution of the envelope of central SLP from the ensemble members and the control run [highest (lowest) values in long (short) dashed lines], central SLP of the control run (thin solid lines), and of the analysis (thick solid lines). Plots for three different initial times are shown for 0000 UTC on (a) 3, (b) 4, and (c) 5 Sep. (A colon replaces the slash for date notation on the abscissa.)

reaches its greatest intensity (964 hPa at 1200 UTC 6 September), the anomalies are virtually collocated and thus can no longer positively interact.

This sequence of events is summarized in Fig. 8. The track of the upper-level PV maximum is represented by the maximum pressure on the 2-PVU surface. The low-level PV maximum, as in Fig. 7, is represented at the 850-hPa level.

Figure 9 compares the minimum SLP to the PV anomaly interaction—shown as the horizontal separation between anomaly centers. The period of explosive intensification begins when the anomaly centers come within 700 km of each other. A 700-km separation is maintained throughout the intensification period, and it is not until the separation distance decreases to about 200 km that we observe the end of the intensification. This is the phase-locking discussed by Hoskins et al. (1985). By analyzing differences between the ensemble members in the next section, we see that the wrapping process and this PV interaction play a crucial role in Earl's reintensification.

5. Diagnosis of CMC ensemble forecasts

a. General performance of the CMC operational ensemble forecasting system

The CMC operational ensemble forecasting system consists of eight SEF members and one control run. As mentioned in section 1, forecasts from three different initial times (0000 UTC on 3, 4, and 5 September) were examined in detail. Since this system includes the effects of both different initial conditions and different model configurations for the ensemble members, it reflects the uncertainties arising from both the initial conditions and the model errors (Wilson et al. 1999).

Figure 10 shows the time evolution of the upper

boundary and lower boundary of the central SLP from the ensemble members, the control run, and the regional analysis. We define the upper and lower boundaries of the central SLP as the highest and lowest values among the ensemble members (including the control run), respectively.

The results of our analysis for runs initialized at 0000 UTC 3 September appear in Fig. 10a. The differences in SLP at the initial time are a result of the different conditions used for each ensemble. The spread between the lowest and highest SLP values increases significantly after 1200 UTC 4 September, just prior to the weakest stage of the system. The control run performs poorly until 0000 UTC 5 September, with values close to that of the upper boundary. Thereafter, the control approximates the midpoint between the upper and lower boundaries. Not even the lowest SLP of the members comes close to the actual minimum SLP of 964 hPa at 1200 UTC 6 September.

For the integrations initialized at 0000 UTC 4 September (Fig. 10b) no member deepens the cyclone below 982 hPa. In fact, many of the members ''lost'' Earl during this integration, which was initialized at a time when the low-level PV anomaly was quite weak (Fig. 6d). Two criteria were used to decide whether the ensemble member failed to follow the original surface cyclone: 1) if no such closed center could be determined based on 4-hPa sea level pressure analyses or 2) the center was discernible but the 1000–500-hPa thickness over the center decreased by 15 dam over a 12-h period. The latter case is one in which the model suggests a secondary cyclogenesis by ''jumping'' from the remnant tropical cyclone to a purely extratropical cyclone without undergoing transition.

Figure 10c displays the results for integrations initialized at 0000 UTC 5 September. The spread between
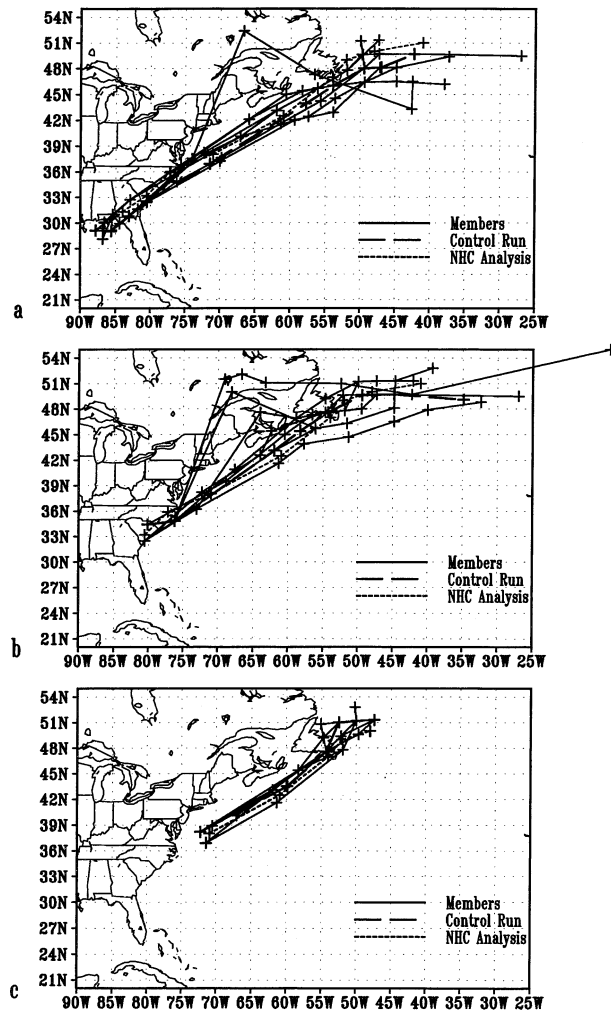
FIG. 11. Model tracks for all ensemble members (1–8) initialized at 0000 UTC on (a) 3, (b) 4, and (c) 5 Sep (solid). Also included are the NHC best tracks (short dashed) and the control run results (long dashed). All tracks are plotted at 12-h intervals from their initialization times to 1200 UTC 7 Sep [except for (c), in which the final time is 0000 UTC 7 Sep].

understand the superior performance of some members, particularly those initialized at 0000 UTC 5 September.

b. Characteristics of the ensemble means

For integrations initialized at 0000 UTC 5 September, the means of the 1000–500-hPa geopotential thickness over the center, the maximum dynamic tropopause pressure, and the low-level PV are plotted in Fig. 12. The results are collected into three groups according to minimum SLP: those less than or equal to 977 hPa (group 1, solid lines), those greater than or equal to 985 hPa (group 2, short dashed lines), and those between 985 and 977 hPa (group 3, long dashed lines). Members that deepened the cyclone the most, as reflected by a stronger low-level PV anomaly during the reintensification period, had a better representation of the remnant tropical air mass (as evidenced by a large 1000–500-hPa thickness) and stronger upper-level PV anomalies (larger values of maximum pressure on the 2-PVU surface).

A similar conclusion can also be drawn from examining the mean behavior of the ensembles that were run from the three different intital times. The minimum SLP valid at 1200 UTC 6 September from the runs with initial time of 0000 UTC on 3 (84-h forecasts, short dashed), 4 (60-h forecasts, long dashed) and 5 September (36-h forecasts, solid) are plotted in Fig. 13a. Clearly the SLP values in the runs originating at 0000 UTC 5 September are generally the lowest, while those from the runs originating at 0000 UTC 4 September are generally the highest. The remaining panels in Fig. 13 examine the mean properties of the members that tracked the former Earl throughout its entire life cycle from the three initial times: the control run and members 2, 4, 5, and 7. Figures 13b–d display the mean thickness over the minimum SLP center, the mean lower-level PV, and the mean maximum pressure on the 2-PVU surface for the above five members together with the regional analysis, respectively. The results for the runs initialized at 0000 UTC 4 September (long dashed) illustrate that their less intense SLP centers correspond with lower thickness, lower pressure on the 2-PVU surface, and smaller low-level PV. These figures also reveal that the integrations initialized at 0000 UTC 5 September (thin solid), which had the most intense SLP centers among the forecasts from the three different initial times, also had stronger anomalies in lower- and upper-level PV. Compared to the analyses, the forecasts initialized at 0000 UTC 3 September (short dashed) overpredicted the warm anomaly (larger thickness) over the SLP centers from 0000 UTC 3 September to 0000 UTC 5 September. These forecasts also had the highest thicknesses among the forecasts made from the three different initial times. This is one of the reasons that the integrations initialized at 0000 UTC 3 September reached lower central SLP values than did the integrations initialized at 0000 UTC 4 September.

The runs that contained the most accurate initial rep-

lower and upper SLP boundaries is the smallest for this run, which reflects the fact that the PV anomaly interaction was beginning near this time. There seems to be more of a consensus between the runs as to the nature of the reintensification.

Composites of the model tracks are displayed in Fig. 11 for integrations initialized at 0000 UTC on each of 3, 4 and 5 September, along with the NHC best track and the control run. A number of runs, especially those initialized at 0000 UTC 4 September, lose the remnant tropical cyclone and produce a jump in position. A tighter clustering of tracks for the 0000 UTC 5 September run in Fig. 11c is observed, yet most are north of the official storm track. This initialization also yields better agreement between members on the position of the storm at 1200 UTC 6 September.

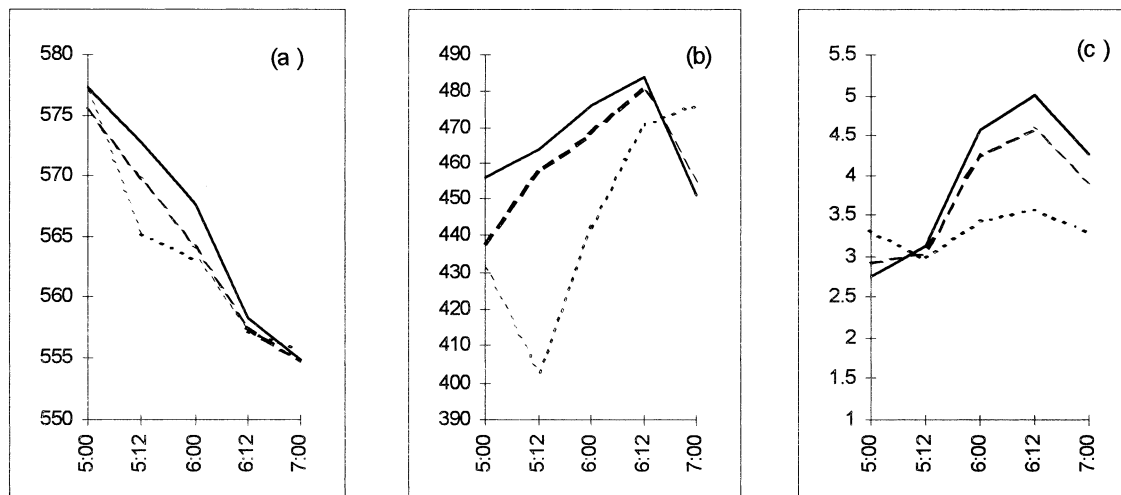We now turn to a more detailed diagnosis to better

FIG. 12. For forecasts with initial time 0000 UTC 5 Sep, (a) mean thickness over the storm center, (b) mean maximum pressure on the 2.0-PVU surface, and (c) mean low-level PV. Solid lines represent ensemble members with SLPs less than or equal to 977 hPa, short dashed lines represent members with SLPs greater than or equal to 985 hPa, and long dashed lines represent members with SLPs between 985 and 977 hPa.

resentation of the tropical air mass and that had the largest values of upper-level PV resulted in the most intense systems as evidenced by large lower-level PV values.

c. Patterns on the dynamic tropopause

Here we compare the evolution of the upper-level PV anomalies of two ensemble members (initialized at 0000 UTC 3 September), one of which does a good job at reintensifying the cyclone (member 1) and the other of which did not perform as well (member 6). In an analysis of the low-level PV anomaly we determined that member 1 resolved this feature much better than did member 6. An analysis of the dynamic tropopause was performed at three periods during the integration. The results are shown in Fig. 14 covering the period from just prior to reintensification to the time when the cyclone was weakening on 7 September. The locations and central pressures of the associated surface lows are also indicated. After 72 h of integration, the anomaly of member 1 appears to be sharper than that of member 6. This is interpreted as a sharpened midlevel trough that fuels the observed cyclogenesis in member 1 through enhanced vorticity advection. After 96 h, the anomaly of member 1 has wrapped into a classic hook structure similar to the feature discussed by Browning et al. (1998) and seen clearly in the PV field at 300 hPa (Fig. 7). Although member 6 shows a hint of this PV wrapup, it is much less dramatic.

Figure 15 shows the pressure on the 2-PVU surface from selected ensemble members initialized at 0000 UTC 3 September and 0000 UTC 5 September, along with the regional analysis and the control run. Each chart is valid for the 12-h period when the member reached its minimum SLP before 1200 UTC 7 September. The

wrapping-up process (such that the 250-hPa contour threshold wraps north of the maximum pressure center) was best simulated by members 1 and 3, and the control initialized at 0000 UTC 3 September, and by members 2, 3, 6, and 8, and the control initialized at 0000 UTC 5 September. Each of these members achieved a minimum sea level pressure less than or equal to 980 hPa. In reaching 974 hPa, member 2 simulated the strongest reintensification.

d. Potential vorticity inversions

To better document the importance of PV dynamics in determining which members best captured Earl's reintensification, PV inversions were performed on the forecasts initialized at 0000 UTC 5 September.

To quantify the dynamics associated with each of the major positive PV anomalies in the ensemble members, we applied the piecewise PV inversion technique of Davis and Emanuel (1991). The mean state was based on an 18-day average centered on 0000 UTC 5 September. Dirichlet conditions retaining the full streamfunction and geopotential perturbations were applied at the lateral boundaries. Inversions performed using homogenous Neumann conditions yielded identical results away from the immediate boundary areas. Twelve levels (1000, 925, 850, 700, 500, 400, 300, 250, 200, 150, 100, 50 hPa) were used for the inversion, with the top and bottom boundary conditions supplied by the 50- and 1000-hPa perturbation potential temperatures, respectively.

Figure 16 presents 24-h forecasts of the 1000–850-hPa thickness advection calculated using the component velocities attributable to the upper-level dry PV anom-
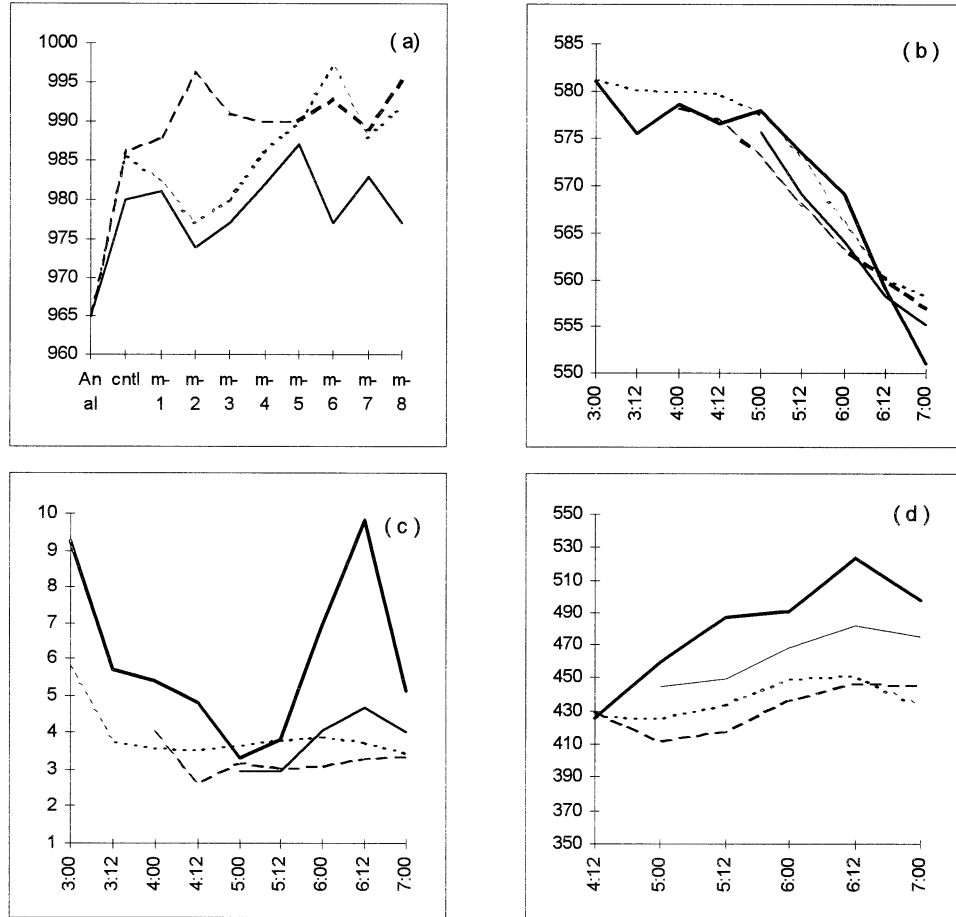
FIG. 13. Selected fields from selected ensemble members for initial time at 0000 UTC on 3, 4, and 5 Sep. (a) Sea level pressure at 1200 UTC 6 Sep for the analysis, control run, and all the ensemble members with initial time at 0000 UTC on 3 (short dashed), 4 (long dashed), and 5 Sep (solid). (b) Mean thickness over the center, (c) mean low-level PV, and (d) mean maximum pressure on the 2-PVU surface. In (b)–(d) thick solid lines are for regional analysis, short dashed lines are for initial time 0000 UTC 3 Sep, long dashed lines for initial time 0000 UTC 4 Sep, and thin solid lines for initial time 0000 UTC 5 Sep.

aly[1] from 0000 UTC 5 September. Contours are plotted in intervals of 2×10^{-3} m s^{-1} with the +1, +2, and +3 $\times 10^{-3}$ m s^{-1} areas shaded to represent regions of positive thickness advection produced by the upper-level dry PV anomaly. Figure 16 thus presents the low-level dynamical impact attributable to the upper-level PV anomaly. Here we see that the members that successfully captured the wrapping-up process and Earl's reintensification (the control run and members 2, 3, 6, and 8) all had maximum values of 5.4 m s^{-1} or higher, whereas the unsuccessful members (with the exception of member 4) had lower values. Member 2 had the strongest value of this diagnostic and also generated the strongest cyclone. The inverted lower-tropospheric winds associated with the upper anomalies (not shown)

reveal stronger couplets of thermal advection in the more successful members.

6. Summary and conclusions

The factors governing the extratropical reintensification of a remnant tropical system south of Newfoundland—Hurricane Earl, September 1998—have been studied using the Canadian Meteorological Centre regional analysis and ensemble forecast system. The transition phase of Hurricane Earl's life cycle began soon after landfall at 0600 UTC 3 September, and NHC declared the storm extratropical at 1800 UTC 3 September. Earl's decay continued as the storm moved off the North Carolina coast and curved cyclonically to track parallel to the East Coast of the United States about 400 km offshore. By 0000 UTC 5 September, the weakened system (now filled to 1004 hPa) lay off the New Jersey coast but was beginning to accelerate northeastward un-

---

[1] Defined as any positive PV anomaly at or above 850 hPa whose relative humidity is 30% or less.
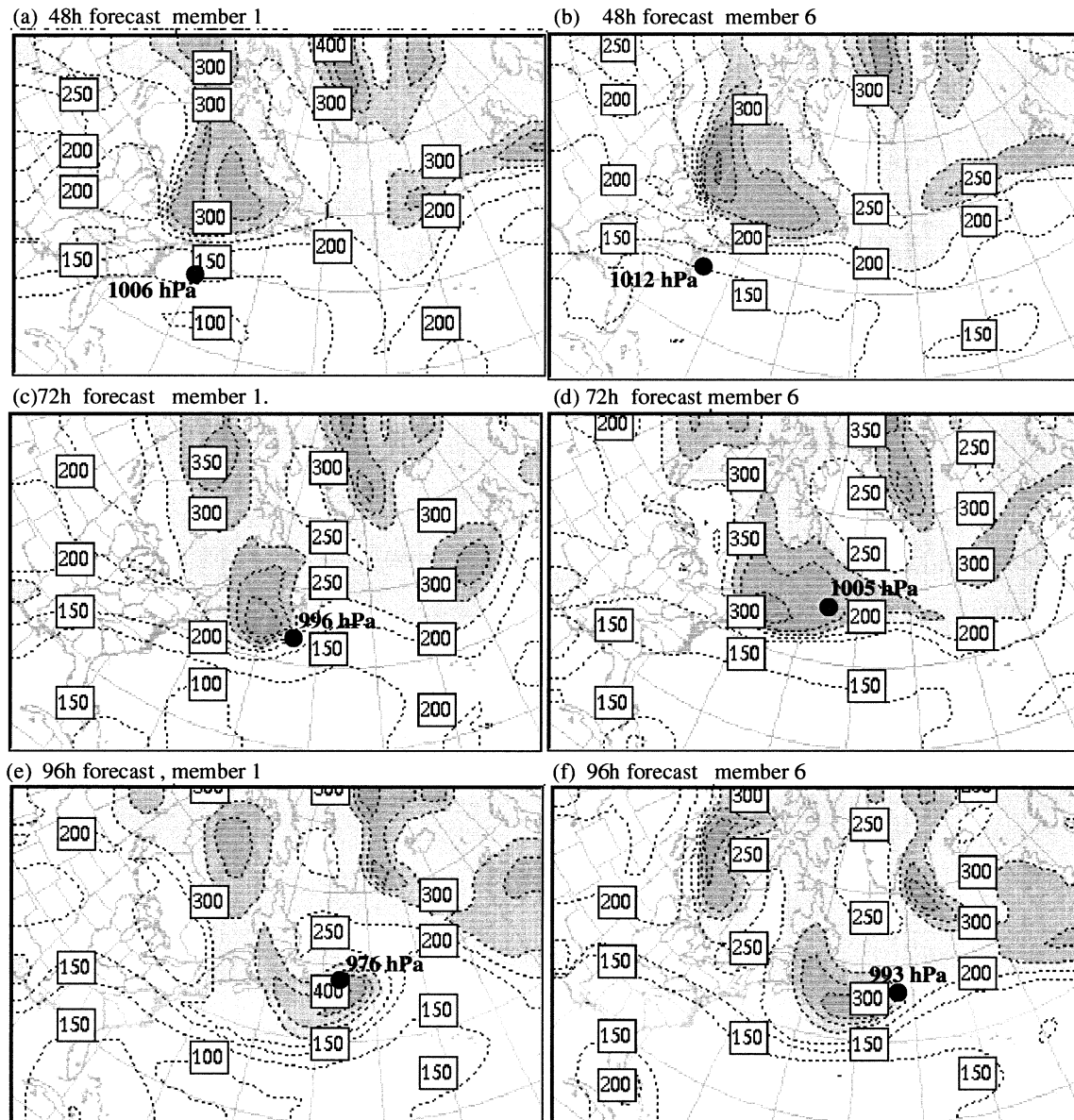
FIG. 14. Pressure on the 2-PVU surface for ensemble members 1 and 6. Plots are shaded for pressures greater than 250 hPa (depressed tropopause). Both members were initialized at 0000 UTC 3 Sep, thus, (a), (c), (e) and (b), (d), (f) correspond to the 48-, 72-, and 96-h forecasts of members 1 and 6, respectively. Locations and central pressures of corresponding surface lows are indicated in boldface.

der the influence of an approaching upper-level trough. Through deformation of the coastal baroclinic zone, strong frontal features began to appear shortly after that time, and the SLP of the reintensifying system began to drop rapidly. Deepening 40 hPa during its 36-h extratropical reintensification phase, the former Earl produced heavy precipitation over Nova Scotia before making landfall on Newfoundland's Avalon Peninsula at 1200 UTC 6 September as a 964-hPa low with 25 m s^{-1} winds. The system entered a second decay phase shortly thereafter, and tracked eastward until 1800 UTC 8 September when it was absorbed into the long-lived

extratropical cyclone resulting from the transition of Hurricane Danielle.

Using a PV perspective for the case diagnosis and static PV inversions, it was found that the factors necessary for the reintensification of the remnant tropical system were (a) the presence of a strong upper-level dry positive PV anomaly and warm, moist low-level diabatically generated PV anomaly and (b) an interaction between the two PV anomalies such that they underwent mutual intensification for an extended period of time. The interaction between anomalies was shown to occur when the upper-level PV anomaly wrapped about the
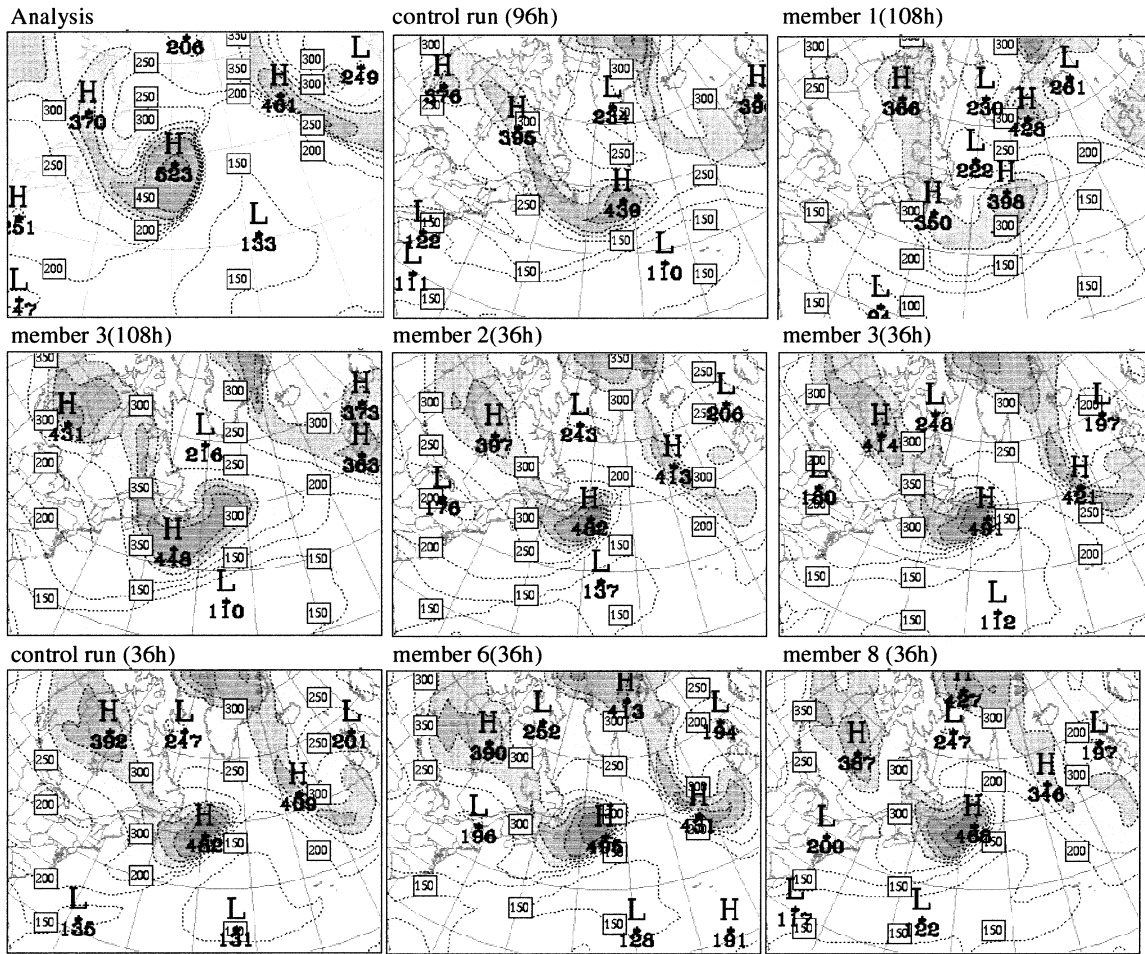
FIG. 15. Pressure on dynamic tropopause (2-PVU surface) for selected ensemble members with initial time of 0000 UTC on 3 and 5 Sep, control run and analysis. The analysis is valid at 1200 UTC 6 Sep and the number in the brackets is the length of the forecast. All are valid for the 12-h period when they reached their minimum sea level pressure up to and including 1200 UTC 7 Sep. Unit, hPa; interval, 50 hPa, with pressure greater than 250 hPa shaded.

lower-level PV anomaly in a cyclonic fashion while maintaining a horizontal separation of about 700 km during the reintensification period, which is consistent with the phase-locking theory of Hoskins et al. (1985).

Results from the study of the eight-member ensemble forecast system showed that (a) integrations initialized at 0000 UTC 4 September resulted in the greatest number of members failing to continuously track the remnant tropical system, (b) there was much greater consensus between members initialized at 0000 UTC 5 September, and (c) the members that best resolved the upper and lower PV anomalies (i.e., had the largest central PV values and sharpest shape definition) yielded the lowest SLPs at maximum intensity.

Accurately predicting the extratropical transition of tropical cyclones remains a forecasting challenge. Even more difficult, however, is predicting in real time whether these systems will subsequently reintensify explosively. The results of this study suggest a knowledge of the strength and positioning of the upper and lower pos-

itive PV anomalies is crucial for the accurate forecasting of these events. Strong PV anomalies separated by a horizontal distance of less than 1000 km may be candidates for phase locking and rapid reintensification of the type described in this case study. It is our hope that these results will help to focus further research on the topic of extratropical transition and will improve the operational predictability of these potentially damaging events.
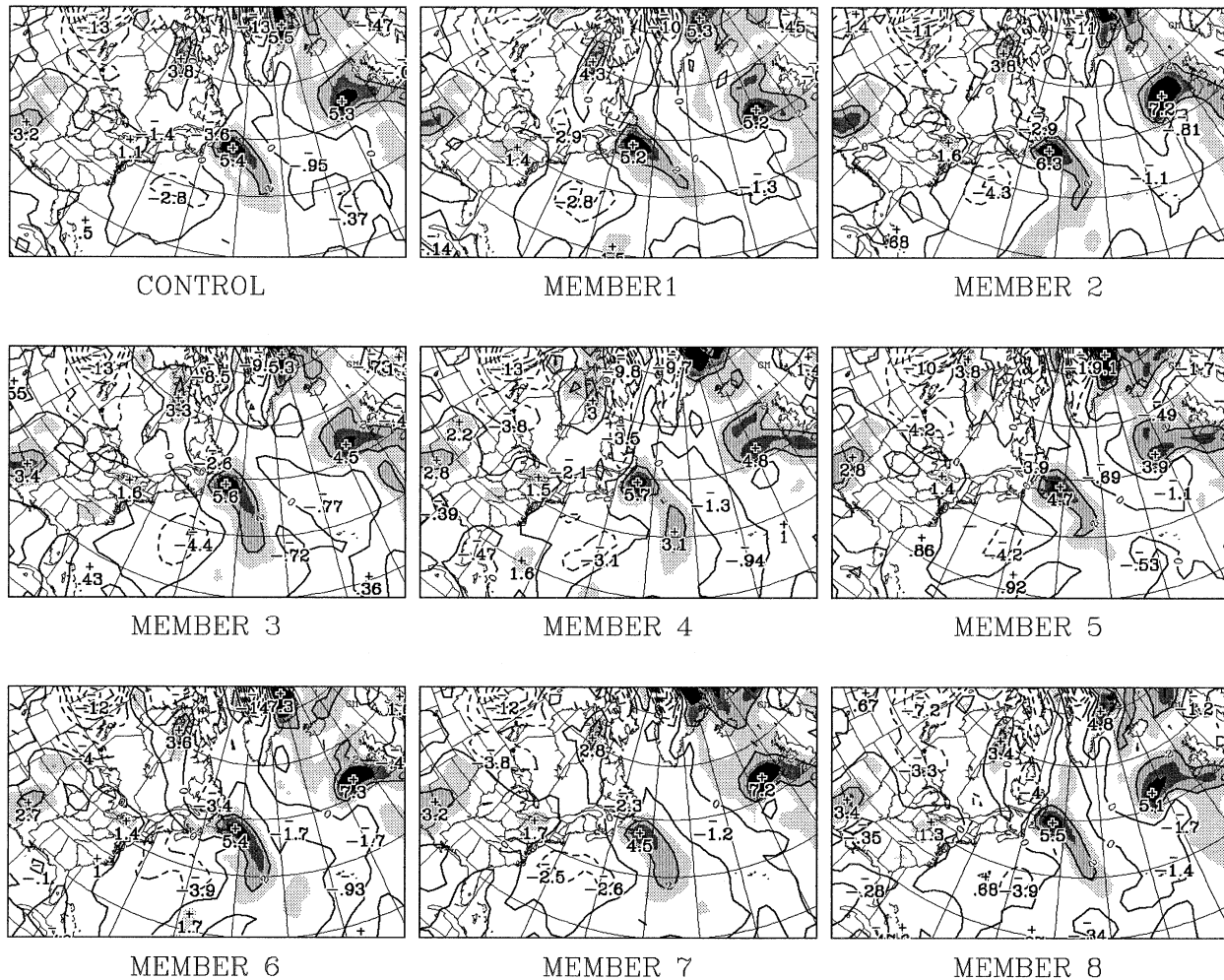
SEF 1000-850 THICKNESS ULDPVA

FIG. 16. The 24-h forecast of 1000–850-hPa thickness advection calculated using component velocities attributable to the upper-level dry PV anomaly from the 0000 UTC 5 Sep SEF ensemble run. Contours are plotted in intervals of 2×10^{-3} m s^{-1} with the $+1$, $+2$, and $+3$ $\times 10^{-3}$ m s^{-1} areas shaded to represent regions of warm thickness advection caused by the upper-level dry PV anomaly.

REFERENCES

Anthes, R. A., 1982: *Tropical Cyclones—Their Evolution, Structure, and Effects. Meteor. Monogr.,* No. 41, Amer. Meteor. Soc., 208 pp.

Browning, K. A., G. Vaughan, and P. Panagi, 1998: Analysis of an ex-tropical cyclone after its re-intensification as a warm core extratropical cyclone. *Quart. J. Roy. Meteor. Soc.,* **124,** 2329–2356.

Davis, C. A., and K. A. Emanuel, 1991: Potential vorticity diagnostics of cyclogenesis. *Mon. Wea. Rev.,* **119,** 1929–1953.

DiMego, G. J., and L. F. Bosart, 1982: The transformation of Tropical Storm Agnes into an extratropical cyclone. Part I: The observed fields and vertical motion computations. *Mon. Wea. Rev.,* **110,** 385–411.

Ertel, H., 1942: Ein neuer hydrodynamischer wirbelsatz. *Meteor. Z.,* **59,** 277–281.

Foley, G. R., and B. N. Hanstrum, 1994: The capture of tropical cyclones by cold fronts off the west coast of Australia. *Wea. Forecasting,* **9,** 577–592.

Hart, R., and J. L. Evans, 2001: A climatology of the extratropical transition of Atlantic tropical cyclones. *J. Climate,* **14,** 546–564.

Holland, G. J., 1993: Ready reckoner. *Global Guide to Tropical Cyclone Forecasting,* G. J. Holland, Ed., World Meteorological Organization WMO/TD-560, 9.1–9.26.

Hoskins, B. J., M. E. McIntyre, and A. W. Robertson, 1985: On the use and significance of isentropic potential vorticity maps. *Quart. J. Roy. Meteor. Soc.,* **111,** 877–946.

Houtekamer, P. L., and L. Lefaivre, 1997: Using ensemble forecasts for model validation. *Mon. Wea. Rev.,* **125,** 2416–2426.

——, ——, J. Derome, H. Ritchie, and H. L. Mitchell, 1996: A system simulation approach to ensemble prediction. *Mon. Wea. Rev.,* **124,** 1225–1242.

Joe, P., and Coauthors, 1995: Recent progress in the operational forecasting of severe weather. *Atmos.–Ocean,* **33,** 250–302.

Jones, B., 1990: Canadian disasters. AES, Ottawa, ON, Canada, 13 pp.

Klein, P. M., P. A. Harr, and R. L. Elsberry, 2000: Extratropical transition of western North Pacific tropical cyclones: An overview and conceptual model of the transformation stage. *Wea. Forecasting,* **15,** 373–395.

Knox, J. L., 1955: The storm "Hazel"—Synoptic resumé of its development as it approached southern Ontario. *Bull. Amer. Meteor. Soc.,* **36,** 239–246.

Lackmann, G., L. F. Bosart, and D. Keyser, 1996: Planetary and synoptic-scale characteristics of explosive wintertime cyclogenesis over the western North Atlantic Ocean. *Mon. Wea. Rev.,* **124,** 2672–2702.

Lawrence, M. B., and B. M. Mayfield, 1998: Atlantic hurricane season of 1995. *Mon. Wea. Rev.,* **126,** 1124–1151.

Mayfield, B. M., 1999: Preliminary report—Hurricane Earl. National Hurricane Center, 8 pp. [Available online at http:// www.nhc.noaa.gov/1998earl.html.]

McTaggart-Cowan, R., J. R. Gyakum, and M. K. Yau, 2001: Sensitivity testing of extratropical transitions using potential vorticity inversions to modify initial conditions: Hurricane Earl case study. *Mon. Wea. Rev.,* **129,** 1617–1636.

Palmén, E., 1958: Vertical circulation and release of kinetic energy during the development of Hurricane Hazel into an extratropical cyclone. *Tellus,* **10,** 1–23.

Pasch, R. J., and L. A. Avila, 1999: Atlantic hurricane season of 1996. *Mon. Wea. Rev.,* **127,** 581–610.

Pierce, C., 1939: The meteorological history of the New England hurricane of Sept. 21, 1938. *Mon. Wea. Rev.,* **67,** 237–288.

Ritchie, H., and C. Beaudoin, 1994: Approximation and sensitivity experiments with a baroclinic semi-Lagrangian spectral model. *Mon. Wea. Rev.,* **122,** 2391–2399.

Rossby, C. G., 1940: Planetary flow patterns in the atmosphere. *Quart. J. Roy. Meteor. Soc.,* **66** (Suppl.), 68–87.

Sanders, F., and J. R. Gyakum, 1980: Synoptic–dynamic climatology of the "bomb." *Mon. Wea. Rev.,* **108,** 1589–1606.

Shapiro, M. A., and D. Keyser, 1990: Fronts, jet streams and the tropopause. *Extratropical Cyclones: The Erik Palmén Memorial Volume,* C. W. Newton and E. O. Holopainen, Eds., Amer. Meteor. Soc., 167–191.

Simpson, R. H., and P. J. Hebert, 1973: Atlantic hurricane season of 1972. *Mon. Wea. Rev.,* **101,** 323–333.

Sinclair, M. R., 1993: Synoptic scale diagnosis of the extratropical transision of a southwest Pacific tropical cyclone. *Mon. Wea. Rev.,* **121,** 941–960.

Thorncroft, C. D., and S. Jones, 2000: The extratropical transitions of Hurricanes Felix and Iris in 1995. *Mon. Wea. Rev.,* **128,** 947–972.

——, B. J. Hoskins, and M. E. McIntyre, 1993: Two paradigms of baroclinic-wave life-cycle behaviour. *Quart. J. Roy. Meteor. Soc.,* **119,** 17–55.

Walmsley, J. L., 1993: The transatlantic fate of tropical storms. *Weather,* **48,** 350–359.

Wilson, L. J., W. R. Burrows, and A. Lanzinger, 1999: A strategy for verification of weather element forecasts from an ensemble prediction system. *Mon. Wea. Rev.,* **127,** 956–970.

Zhang, Z., and T. N. Krishnamurti, 1999: A perturbation method for hurricane ensemble predictions. *Mon. Wea. Rev.,* **127,** 447–469.